Subwavelength grating-mirror VCSEL with a thin oxide gap

Chung, Il-Sug; Mørk, Jesper; Gilet, Philippe; Chelnokov, Alexei

Published in:
IEEE Photonics Technology Letters

Link to article, DOI:
10.1109/LPT.2007.912689

Publication date:
2008

Document Version
Publisher's PDF, also known as Version of record

Subwavelength Grating-Mirror VCSEL With a Thin Oxide Gap

II-Sung Chung, Jesper Mørk, Philippe Gilet, and Alexei Chelnokov

***Abstract*—A new vertical-cavity surface-emitting laser (VCSEL) structure based on a subwavelength grating mirror and a thin oxide gap is suggested and numerically investigated. The structure is shown to exhibit similar threshold gain, suppression of higher order transverse modes, and polarization stability as a grating-mirror VCSEL reported in the literature based on a thick air gap. The thin oxide gap structure has a number of advantages including easier fabrication, better mechanical stability, and very strong single-mode properties.**

***Index Terms*—Grating, high power, single mode.**

I. Introduction

MANY vertical-cavity surface-emitting laser (VCSEL) designs have been reported to improve single-mode output power with or without polarization stability [1]–[5]. A recently reported high index contrast subwavelength grating-mirror (HCG) VCSEL with a $5\lambda/4$-thick air gap is noteworthy due to its unique concept and characteristics [6]. In this design, as is schematically shown in Fig. 1(b), the single layer HCG suspended in the air replaces most of the top distributed Bragg reflector (DBR). This HCG VCSEL demonstrated 25-dB orthogonal polarization suppression ratio and 45-dB sidemode suppression ratio at 0.9-mW output power. The demonstrated ~1-mW output power is much smaller than the state-of-the-art ~7-mW single-mode output power with the same GaAs–AlGaAs quantum-well (QW) system [4], but is expected to be improved by further optimization of thermal design. Thus, this HCG VCSEL design can be an advantageous approach to single-mode high-power VCSELs with polarization stability. Especially, long wavelength VCSELs can benefit from this approach since the wafer-bonded GaAs lattice-matched top DBR can be replaced by an InP lattice-matched grating [7].

In this letter, based on extensive full vectorial simulations, it is suggested that the $5\lambda/4$-thick air gap below the grating in Fig. 1(b) can be replaced by a $\lambda/4$-thick oxide gap, as shown in Fig. 1(c), for ease of HCG fabrication (wet oxidation instead of sacrificial etching) and better mechanical stability [6]. In addition, it is shown that higher order modes can be efficiently suppressed by reducing the area of HCG region. Two aspects need to be considered. 1) The oxide gap below the HCG can be easily formed by wet oxidation because of the large area opened through the corrugation of grating and short oxidation distance (~215 nm for the 1.55-μm wavelength case). Thus, in the oxide-confined VCSEL case, the oxide gap and oxide current aperture can be formed at the same time. 2) This oxide gap HCG can be utilized for InP-based tunnel junction VCSELs as well if an appropriate oxidation compatible InP lattice-matched material is chosen, for instance, as in [8].

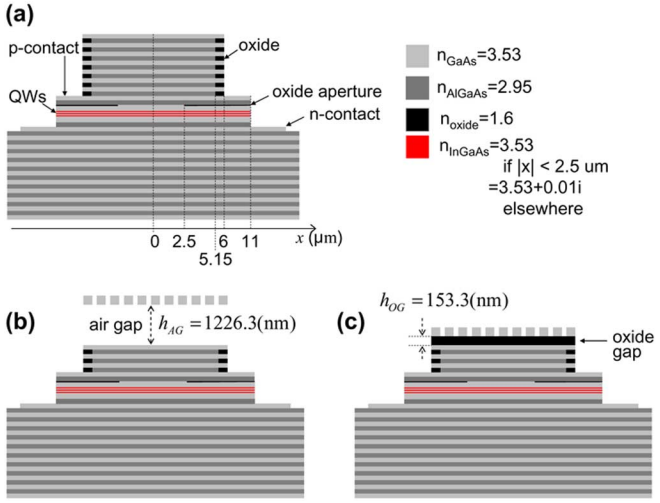

Fig. 1. Schematic diagrams of investigated (a) plain intracavity-contacted VCSEL, (b) HCG VCSEL with a $5\lambda/4$-thick air gap, and (c) HCG VCSEL with a $\lambda/4$-thick oxide gap. In all designs, an oxide aperture layer is located at the anti-node position of longitudinal mode profile. The period $\Lambda_{\rm gr}$, thickness $h_{\rm gr}$, and duty cycle $\Gamma_{\rm gr}$ of gratings in (b) and (c) are 390.8, 244.9, and 0.615 nm, respectively. The size of HCG region in (b) and (c) is 12.1 μm wide.

II. Device Structure and Simulation Method

The investigated VCSEL structure is based on the 980-nm epi design suggested in [9]. The plain VCSEL in Fig. 1(a) consists of a 25-pair GaAs–AlGaAs top DBR, a λ-cavity (containing three 8-nm InGaAs–GaAs QWs), and a 29.5-pair bottom DBR. An intracavity-contacted scheme is assumed and partial oxidation of the AlGaAs layers in the top DBR is included (10% of oxidation rate of the oxide current aperture layer). The top mirrors of HCG VCSELs in Fig. 1(b) and (c) are composed of an HCG, an air/oxide gap, and 4-pair DBR. The length scales and refractive indexes are given in Fig. 1, including mesa and oxide aperture sizes. A $\lambda/20$-thick oxide current aperture layer is situated at the anti-node position of the longitudinal mode profile. The wavelength λ referred to in the device dimensions is 981 nm.

The two-dimensional finite-difference time-domain (FDTD) method with PML boundary condition is used. Our method successfully reproduced the measured reflectivity curve of the HCG mirrors in [10] and the measured threshold gain of the HCG

Manuscript received August 16, 2007; revised September 29, 2007. This work was supported by EU IST-FP6 through the MOSEL Project.

I.-S. Chung and J. Mørk are with the Department of Communications, Optics, and Materials, Technical University of Denmark (COM·DTU), DK-2800 Kgs. Lyngby, Denmark (e-mail: isc@com.dtu.dk).

P. Gilet and A. Chelnokov are with CEA-G Léti MINATEC, Grenoble FR38054, France.

Color versions of one or more of the figures in this letter are available online at http://ieeexplore.ieee.org.

Digital Object Identifier 10.1109/LPT.2007.912689

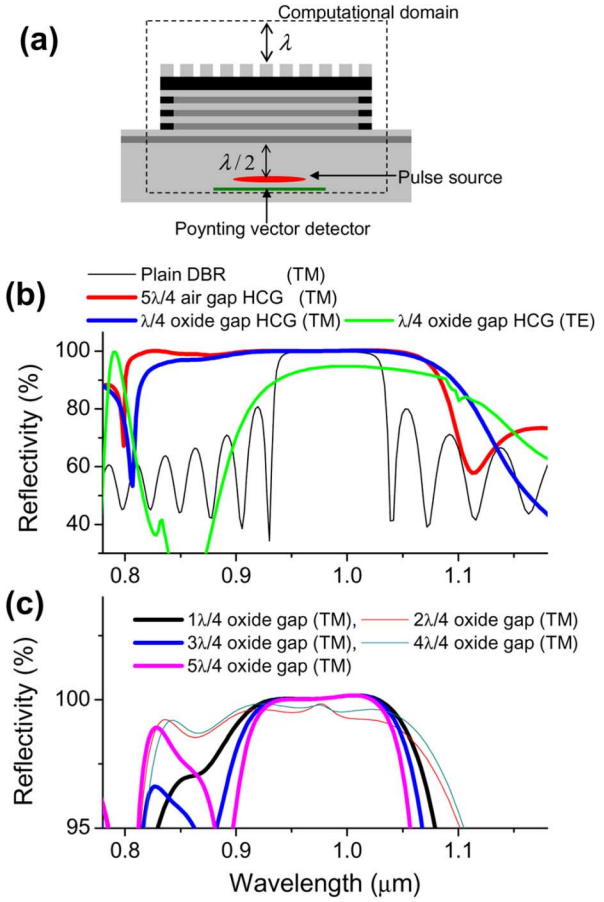

Fig. 2. (a) Schematic diagram of computational domain for reflectivity evaluation: The light source has a temporal Gaussian envelope with a $1/e^2$ width of 1.1 fs ($\lambda/3$ divided by the speed of light), and a spatial Gaussian shape with a $1/e^2$ width of 1.64 μm that is determined by fitting the resonance mode profile at the active region in Fig. 3. The width of the Poynting vector detector just behind the source is the same as the oxide aperture diameter (5 μm). (b) Compares the reflectivities of the plain DBR, $5\lambda/4$-thick air gap HCG, and $\gamma/4$-thick oxide gap HCG. Figure (c) shows the effect of oxide gap thickness on the overall reflectivity of the top mirror.

VCSEL in [6]. Spatial grid sizes for transverse and longitudinal directions are 10.0 and 8.0 nm, respectively. The reflectivities of top mirrors of the three VCSELs in Fig. 1 are obtained by Fourier-transforming the short pulse response and normalizing it with the pulse source spectrum, as schematically shown in Fig. 2(a). The cold cavity threshold gains are obtained by using the following relation [11], [12]:

$$g_{\rm th} = \frac{1}{\Gamma v_g \tau_p} = \frac{-dW/dt}{\Gamma v_g W} \tag{1}$$

where Γ is optical confinement factor, v_g the group velocity, τ_p the photon lifetime, and W the energy stored in the cavity. For a more exact description of mode characteristics, electrical and thermal effects need to be included in the calculation.

III. HCG Mirror

As shown in Fig. 2(b), the transverse-magnetic (TM) polarization (with electric field perpendicular to the grating) reflectivity of the $\lambda/4$-thick oxide gap HCG (HCG $+\lambda/4$-thick oxide gap $+$ 4-pair DBR) is as high as that of the $5\lambda/4$-thick air gap HCG (HCG $+$ $5\lambda/4$-thick air gap $+$ 4-pair DBR), and slightly higher than that of the plain 25-pair DBR at a wavelength of 981 nm. And the bandwidth of TM reflectivity of the $\lambda/4$-thick oxide gap HCG is as broad as that of the $5\lambda/4$-thick air gap HCG. The transverse-electric (TE) polarization (with electric field parallel to the grating) reflectivity of the $\lambda/4$-thick oxide gap HCG is 95% at a wavelength of 981 nm, suppressing the lasing of TE-polarized modes. It is noteworthy that the maximum value and the central wavelength of the reflectivity curve can be engineered by changing the period $\Lambda_{\rm gr}$, duty cycle $\Gamma_{\rm gr}$, and thickness $h_{\rm gr}$ of the grating.

The dependence of TM reflectivity of the oxide-gap HCG on the oxide-gap thickness is shown in Fig. 2(c). The maximum values of TM reflectivities of $\lambda/4$-, $3\lambda/4$-, and $5\lambda/4$-thick cases are almost same, and higher than those of $2\lambda/4$- and $4\lambda/4$-thick cases. The smaller reflectivities of $2\lambda/4$- and $4\lambda/4$-thick cases result from the destructive interference between the reflection from the HCG and those from the 4-pair DBR.

In conclusion, the thinnest $\lambda/4$-thick oxide gap HCG can be as good a mirror as the $5\lambda/4$-thick air gap HCG.

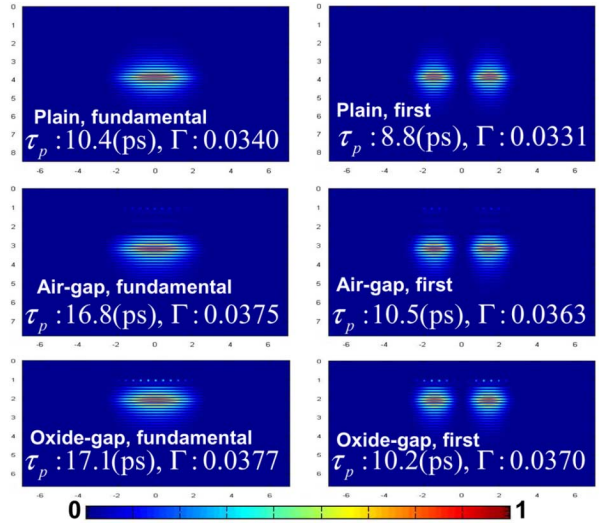

Fig. 3. Normalized mode profile, photon lifetime τ_p, and optical confinement factor Γ of the fundamental and first-order TM-polarized modes of the plain VCSEL, $5\lambda/4$-thick air gap VCSEL, and $\lambda/4$-thick oxide gap VCSEL are listed.

IV. HCG VCSEL

The calculated mode profile and photon lifetime of the fundamental and the first-order TM-polarized modes of the plain VCSEL, air gap VCSEL (with a $5\lambda/4$-thick air gap HCG), and oxide gap VCSEL (with a $\lambda/4$-thick oxide gap HCG) are listed in Fig. 3. In all three cases, the transversal size of the mode profile is determined by the oxide current aperture, due to the oxide aperture layer at the antinode. The photon lifetime, τ_p of the TM-polarized fundamental mode of the oxide-gap VCSEL is similar to that of the air gap VCSEL, as expected from the result of Section III. Slightly higher TM reflectivity of the oxide gap HCG than that of the plain DBR in Fig. 2(b) results in a considerably longer photon lifetime of the oxide gap VCSEL than that of the plain VCSEL. Regarding TE polarization, no resonance is observed, i.e., the photon lifetime of TE modes is close to zero. This result indicates that the $\lambda/4$-thick oxide gap HCG is a high-quality polarization-selective top mirror of VCSEL with

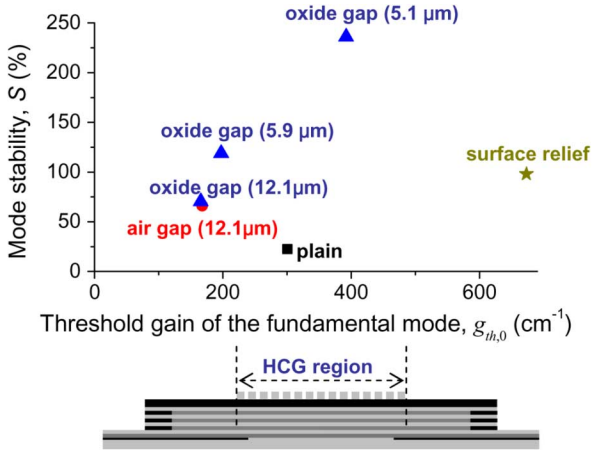

Fig. 4. Mode stability of oxide gap VCSEL is plotted as a function of HCG region size and threshold gain of the fundamental mode. For comparison, an air gap VCSEL with an HCG region size of 12.1 μm, a plain VCSEL, and a surface relief VCSEL with a 5-μm-diameter oxide aperture and 2.5-μm-diameter surface relief [2] are considered. The red and blue lengths in parenthesis indicate the HCG region size of air gap and oxide gap VCSELs, respectively.

properties similar to the $5\lambda/4$-thick air gap HCG. The TM reflectivity of the oxide gap HCG can be adjusted to achieve the desired output power or differential efficiency.

Very strong single-mode characteristics can be achieved by optimizing the HCG region size with respect to the oxide aperture size. The extent of suppression of higher order modes is quantified by the mode stability factor S, defined as [9]

$$S = \frac{g_{\mathrm{th},1} - g_{\mathrm{th},0}}{g_{\mathrm{th},0}} \times 100(\%) \tag{2}$$

where $g_{\mathrm{th},0}$ and $g_{\mathrm{th},1}$ represent the threshold gains of the fundamental and first-order modes, respectively. In Fig. 4, the mode stability factor S of the oxide gap VCSEL increases as its HCG region size is reduced. The preferable HCG region size is 5.1 μm, which gives quite high mode stability and acceptable threshold gain of the fundamental mode. With HCG regions size smaller than the oxide aperture diameter of 5 μm, the threshold gain of the fundamental mode becomes undesirably high.

The mode discrimination of HCG VCSELs relies on a spatial variation of the reflectivity. The reflectivity of HCG is the most efficient in the HCG center and drops by a few tens of percent outside the HCG region. As a result, higher order modes see smaller modal reflectivities than the fundamental mode, i.e., experience much higher modal losses. The mode-discrimination mechanism of surface relief VCSELs is also based on spatially varying reflectivity. However, the magnitude of mode discrimination of HCG VCSELs is much stronger than that of surface relief VCSELs. In HCG VCSELs, the reflectivity difference between the center and edge is tens of percent, e.g., 20%–30% at least. However, in surface relief VCSELs, it is a few percent, e.g., 1%–3% at most. In Fig. 4, the mode stability of an oxide gap VCSEL with a 5.1-μm-wide HCG region is 236% while that of the state-of-the-art surface relief VCSEL design is 98% [2].

For better relaxation of current crowding, the position of p- and n-contact GaAs layers used in [6] is preferable. Whereas, for better heat dissipation through metal contacts, especially in the flip-chip bonding case, the contact position used in this report is advantageous. It is because the thermal conductivity of GaAs–AlGaAs DBR is considerably lower than its average bulk value [13]. The potential reliability problem due to the oxide gap layer being exposed to air needs to be tested and possibly can be avoided by sealing the oxide layer from the environment.

V. Conclusion

A new VCSEL structure based on a subwavelength grating mirror and a thin oxide gap has been investigated and shown to exhibit performance characteristics similar to that of air-gap-based structures suggested in the literature. The oxide-based structure allows much simpler fabrication and has a better mechanical stability. An optimized grating mirror structure allows realizing very strong single-mode properties.

References

[1] D. Zhou and L. J. Mawst, "High-power single-mode antiresonant reflecting optical waveguide-type vertical-cavity surface-emitting lasers," *IEEE J. Quantum Electron.*, vol. 38, no. 12, pp. 1599–1606, Dec. 2002.

[2] Å. Haglund, J. S. Gustavsson, J. Vukučsié, P. Modh, and A. Larsson, "Single fundamental-mode output power exceeding 6 mW from VCSELs with a shallow surface relief," *IEEE Photon. Technol. Lett.*, vol. 16, no. 2, pp. 368–370, Feb. 2004.

[3] R. M. Würtemberg, P. Sundgren, J. Berggren, and M. Hammer, "1.3 μm InGaAs vertical-cavity surface-emitting lasers with mode filter for single mode operation," *Appl. Phys. Lett.*, vol. 85, no. 21, pp. 4851–4853, Nov. 2004.

[4] A. Furukawa, S. Sasaki, M. Hoshi, A. Matsuzono, K. Moritoh, and T. Baba, "High-power single-mode vertical-cavity surface-emitting lasers with triangular holey structure," *Appl. Phys. Lett.*, vol. 85, no. 22, pp. 5161–5163, Nov. 2004.

[5] W. Jiang, J. Ramdani, and M. S. Lebby, "Vertical cavity surface emitting laser for high power single mode operations has an extended cavity structure promoting high modal loss," U.S. Patent US6026111-A.

[6] M. C. Y. Huang, Y. Zhou, and C. J. Chang-Hasnain, "A surface-emitting laser incorporating a high-index-contrast subwavelength grating," *Nature Photon.*, vol. 1, pp. 119–122, Feb. 2007.

[7] V. Jayaraman, M. Mehta, A. W. Jackson, S. Wu, Y. Okuno, J. Piprek, and J. E. Bowers, "High-power 1320-nm wafer-bonded VCSELs with tunnel junctions," *IEEE Photon. Technol. Lett.*, vol. 15, no. 11, pp. 1495–1497, Nov. 2003.

[8] S.-J. Bae, J.-M. Kim, C.-Y. Park, and Y.-T. Lee, "Characteristics of InAlAs/InP and InAlP/GaAs native oxides," *Solid State Electron.*, vol. 50, pp. 1625–1628, 2006.

[9] P. Bienstman, R. Baets, J. Vukusic, A. Larsson, M. J. Noble, M. Brunner, K. Gulden, P. Debernardi, L. Fratta, G. P. Bava, H. Wenzel, B. Klein, O. Conradi, R. Pregla, S. A. Riyopoulos, J.-F. P. Seurin, and S. L. Chuang, "Comparison of optical VCSEL models on the simulation of oxide-confined devices," *IEEE J. Quantum Electron.*, vol. 37, no. 12, pp. 1618–1631, Dec. 2001.

[10] C. F. R. Mateus, M. C. Y. Huang, L. Chen, C. J. Chang-Hasnain, and Y. Suzuki, "Broad-band mirror (1.12–1.62 μm) using a subwavelength grating," *IEEE Photon. Technol. Lett.*, vol. 16, no. 7, pp. 1676–1678, Jul. 2004.

[11] L. A. Coldren and S. W. Corzine, *Diode Lasers and Photonic Integrated Circuits*. Hoboken, NJ: Wiley, 1995, ch. 5 and A5.

[12] J. T. Verdeyen, *Laser Electronics*, 3rd ed. Englewood Cliffs, NJ: Prentice-Hall, 1995, ch. 6.

[13] J. Piperk, T. Tröger, B. Schröter, J. Kolodzey, and C. S. Ih, "Thermal conductivity reduction in GaAs–AlAs distributed Bragg reflectors," *IEEE Photon. Technol. Lett.*, vol. 10, no. 1, pp. 81–83, Jan. 1988.